Journal of Membrane Science 328 (2009) 165–173

Contents lists available at ScienceDirect

Journal of Membrane Science

journal homepage: www.elsevier.com/locate/memsci

Mixed-matrix membranes containing MOF-5 for gas separations

Edson V. Perez, Kenneth J. Balkus Jr., John P. Ferraris, Inga H. Musselman*

Department of Chemistry and the Alan G. MacDiarmid NanoTech Institute, The University of Texas at Dallas, Richardson, TX 75080, United States

ARTICLE INFO

Article history:
Received 30 December 2007
Received in revised form
30 November 2008
Accepted 1 December 2008
Available online 7 December 2008

Keywords:
Mixed-matrix membranes
Metal–organic frameworks
MOF-5
Matrimid®
Gas separations

ABSTRACT

Metal–organic framework 5 (MOF-5) nanocrystals with a high surface area (3000 m^2/g) and high thermal stability (up to 400 °C) were synthesized and added to Matrimid® to form mixed-matrix membranes for gas separations. Scanning electron microscopy (SEM) images of the membrane cross-sections revealed significant plastic deformation of the polymer matrix owing to the strong affinity between the MOF-5 and Matrimid®. At 30% MOF-5 loading, the permeabilities of the gases tested increased 120% while the ideal selectivities remained constant compared to Matrimid®. Residual gas analysis of permeates of gas blends with different mixture ratios revealed an increase in selectivity for CH_4.

1. Introduction

As polymer-based gas separations have seemingly reached the limit of the permeability-selectivity tradeoff reported by Robeson [1], new materials and procedures for membrane fabrication are being investigated in order to improve performance. Inorganic membranes have been used widely due to their high permeability and selectivity [2,3]; however, elaborate manufacturing procedures (e.g. support treatment, zeolite crystallization, thermal programming for pyrolysis, and a controlled inert gas atmosphere in terms of flow, pressure, and composition [2–5]), low reproducibility of properties [6], high cost [7], and low mechanical resistance make their production difficult. These technical difficulties and other problems inherent to inorganic membranes are reviewed by Julbe [3] and Saracco et al. [8]. In contrast, polymer membranes incur lower manufacturing costs and have higher mechanical resistance, but they have comparatively low permeability and selectivity making them less attractive than inorganic membranes for gas separations. As an alternative to inorganic and polymer membranes, mixed-matrix membranes (MMM) [9] have begun to attract the attention of researchers. These hybrid membranes combine the superior permeability and selectivity of inorganic membranes with the processability of polymer membranes; additionally, MMMs are mechanically more resilient than inorganic membranes. Other important features that MMMs possess are more reproducible properties and facile [10] and low cost of fabrication. Compared to inorganic membranes, where the membrane cost per m^2 is on the order of thousands of dollars [7], MMMs using metal–organic frameworks (MOFs) could reduce the cost by an order of magnitude [11].

MMMs, however, are not exempt from challenges. The low affinity of the polymer for the inorganic additive can result in the formation of non-selective voids at the polymer–additive interface that degrade the performance of the membrane [12,13]. Evidence of poor wetting by the polymer and debonding of the additives has been presented in scanning electron microscopy (SEM) images of membrane cross-sections [13–15] and polymer composites [16,17]; in these images, little or no plastic deformation of the polymer matrix at the additive–polymer interface is observed owing to poor contact between the organic and inorganic phases. Attempts to fabricate MMMs using zeolites, which are ideal gas separation candidates due to their thermal stability and separation and transport properties, proved to be problematic owing to their inadequate interaction with the polymer and, in some cases, behavior as fillers [15,18–20]. Another challenge that MMMs could face is partial blockage of the additive pore by polymer chains rendering the additive as a filler. This result was observed in a recent study of zeolites 3A, 4A, and 5A in polyethersulfone MMMs in which the permeabilities of the gases decreased with additive loading. Only zeolite 5A reached constant (still lower than the pure polymer) permeability for H_2 and O_2 above a 20% zeolite loading [14]. Mesoporous MCM-41 was employed as an additive in order to enhance the polymer–additive interaction through polymer chain penetration of the mesopores [21]. In terms of interaction, this strategy proved

* Corresponding author. Tel.: +1 972 883 2706; fax: +1 972 883 2925.
E-mail address: imusselm@utdallas.edu (I.H. Musselman).

0376-7388/$ – see front matter © 2008 Elsevier B.V. All rights reserved.
doi:10.1016/j.memsci.2008.12.006

to be effective. Gas separation studies of MCM-41/polysulfone MMMs demonstrated that gas permeability increased with an increased loading of MCM-41 while the selectivity remained constant. The large pores of this material may be easily blocked by the polymer chains leaving the inner pores inaccessible.

Based on the above-mentioned challenges that MMMs face, we have looked for alternative additives that could help mitigate these problems and increase membrane performance. The incorporation of metal–organic frameworks into a polymer matrix for the fabrication of MMMs for gas separations, first explored by Yehia et al. [22] with the incorporation of copper(II) biphenyl dicarboxylate-triethylenediamine in poly(3-acetoxyethylthiophene), showed improvements in CH_4 selectivity. From this pioneering work, we found that MOFs are good candidates as additives for gas separation since they consist of a combination of an inorganic cluster (also known as a secondary building unit or SBU) and an organic bridge [23,24]. This combination of inorganic and organic components increases enormously the variety of MOFs that could be employed in the fabrication of MMMs; virtual libraries of SBUs, based on metals and ligands, have been built based on molecular modeling studies [25]. These libraries could become very important in the selection of proper SBUs for the synthesis of crystals targeting gas separations, once the effective combinations of metals and organic linkers are determined for specific gas pairs. More recently, MOFs have been used successfully in the separation of CO_2/CH_4 by pressure swing adsorption taking advantage of the differences in sorption/desorption pressures of the gases in the MOF and of the large storage capacity of the same [26].

Metal–organic frameworks have been studied extensively mainly for three reasons. First, these materials possess high surface areas (e.g. MOF-177 = 4500 m^2/g [27], MOF-5 = 3000 m^2/g [28,29], and Cu-MOF = 3200 m^2/g [30]) and controlled porosity, which makes them good candidates for gas storage [31] and catalysis [32]. Second, some MOFs may have affinity for certain gases and, therefore, could be used in gas separation (e.g. Seki's Cu-MOF that has a methane sorption capacity of 212 $cm^3_{STP}\,g^{-1}$, which is superior to the sorption capacity of zeolite 5A and nearly the same as activated carbon AX-21 [30]). Third, MOFs are highly flexible in terms of chemical composition, allowing the addition of functional groups that could change the pore size and chemical properties of the MOF [33]. The potential benefits that MOFs could bring to MMMs depend largely on a thorough examination and demonstrated reproducibility of the MOF properties [34,35]. For example, high temperature resistance is a critical property of a MOF that is subjected to high annealing temperatures to remove casting solvent from a mixed-matrix membrane. These high temperatures are required because of the strong interaction between MOFs and certain solvent molecules. For example, Huang et al. have shown that MOF-5 nanoparticles can retain H_2O up to 162 °C, that ethanol is desorbed at 192 °C, and that other organic solvents, such as toluene and xylene, have shown similar increases (40 and 27 °C, respectively) in desorption temperatures above their boiling points [36].

Recently, Yaghi et al. have reported a series of MOFs based on zinc SBUs of which IRMOF-1 or MOF-5 (Fig. 1) presented a high H_2 storage capacity (4.5 wt%) at liquid N_2 temperature suggesting affinity for H_2. This high sorption capacity is attributed to the high surface area of the MOF and to interactions between H_2 and the inorganic cluster and the organic bridge (the two main sorption areas that were detected by inelastic neutron scattering [29,37] and by molecular modeling [38,39]). Molecular dynamics simulations concluded that molecular diffusion in MOF-5 was comparable to that in zeolites and, due to the larger pore size of MOF-5, was most likely attributed to both Knudsen and surface diffusion [40]. These results indicate that the organic linker of the MOF may play a role in the diffusion of gas molecules in addition to interacting with the polymer. MOF-5 is made from Zn_4O clusters linked by three 1,4-benzenedicarboxylate molecules. It exhibits a cubic three-dimensional structure with a pore size of 8 Å that holds a volume equivalent to a surface area of 3000 m^2/g (surface area in these materials arise from pore filling by the probe molecule). MOF-5 nanocrystals possess high thermal stability (up to 400 °C) which expands the use of MOF-5 in membrane fabrication [41].

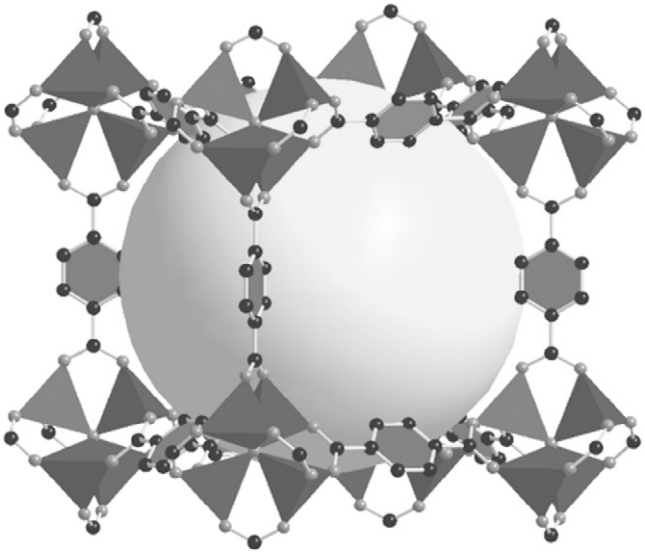

Fig. 1. MOF-5 crystal structure generated from single crystal X-ray diffraction data [28].

In this work, MOF-5 nanocrystals were incorporated into a polymer matrix for the separation of gases and binary mixtures. In addition, the synthesis procedure for MOF-5 nanocrystals was improved to solve the problem of zinc salt hydration that can lead to the formation of two distinct crystal phases. The properties of the nanocrystals are highly reproducible and comparable to those reported in the literature [28,41,42]. Because high thermal stability of the polymer is desired in order to remove casting solvent from the pores of the crystal [15], Matrimid® 5218 (T_g = 350 °C) was chosen; additionally, this polymer is commercially available and its permeability and selectivity properties have been reported elsewhere in the literature. Fig. 2 shows the structure of this polyimide. The membranes were characterized by SEM, powder X-ray diffraction (XRD), thermogravimetric analysis (TGA), and gas permeation.

2. Experimental

2.1. Materials

Benzene-1,4-dicarboxylic acid (BDA, >99%) and zinc nitrate hexahydrate ($Zn(NO_3)_2{\cdot}6H_2O$, >99%) were obtained from Fluka and used without further treatment. $Zn(NO_3)_2{\cdot}6H_2O$ was stored under nitrogen to reduce exposure to moisture. HPLC grade water was obtained from Fisher and used as received. 4A molecular sieves 4–8 mesh (Sigma–Aldrich) were washed with HPLC grade water,

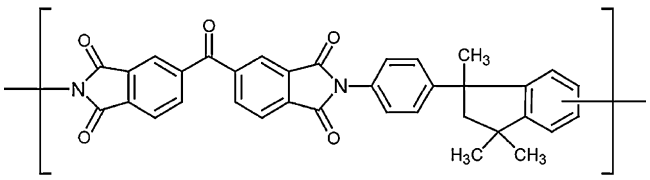

Fig. 2. Structure of Matrimid® 5218.

activated at 400 °C for 1 d, cooled to room temperature in a vacuum oven at low pressure, and stored in capped bottles filled with nitrogen for later use. Chloroform (99.9%, H_2O <0.002%) and acetone (99.7%, H_2O = 0.3%) were purchased from Fisher; *N*,*N*-dimethylformamide (DMF, 99.8%, H_2O <0.15%) was obtained from EMD; triethylamine (TEA, 99%) and anhydrous *N*-methyl-2-pyrrolidone (NMP, 99.5%, H_2O <0.005%) were acquired from Aldrich. All organic solvents were dried over activated 4A molecular sieves for 1 d before use. Matrimid® 5218 was acquired from Ciba Specialty Chemicals, dried at 240 °C for 1 d in a vacuum oven, and stored in nitrogen before use. For membrane casting, Mylar® A92 sheets were purchased from Active Industries. For the permeation experiments, nitrogen, oxygen, hydrogen, methane, carbon dioxide, and their certified mixtures H_2/CO_2 (75/25, 50/50, 25/75), CH_4/N_2 (94/6, 50/50, 25/75), and CH_4/CO_2 (90/10, 50/50, 25/75) were obtained from Air Liquide. The purity of the gases was greater than 99.5% for CH_4 and O_2; the rest of the gases were greater than 99.99% pure.

2.2. Synthesis of MOF-5 nanocrystals

Metal–organic framework 5 (MOF-5) nanocrystals were synthesized in gram quantities by modifying published procedures [36,41,43] to control the water content in the reaction mixture. This procedure can be easily scaled up to larger quantities. In a typical synthesis, 4.00 g (13.50 mmol) of $Zn(NO_3)_2{\cdot}6H_2O$ was dissolved in 250 mL of DMF in a round bottom flask. To remove the excess water adsorbed by the zinc salt, 12.8 g of activated 4A molecular sieves 4–8 mesh were added to the DMF solution. After drying for 1 h, the molecular sieves were removed and then BDA (1.30 g, 7.80 mmol) was added to the DMF solution. The solution was heated to 70 °C and, under strong agitation, TEA (5.05 g, 50.50 mmol) was added drop wise over the course of 10 min to produce a white precipitate; the solution was then left to react for 10 min and cooled to room temperature while stirring continuously. As-synthesized MOF-5 nanocrystals were obtained by filtering the white solution and then washing the white powder with three 30 mL aliquots of DMF. The white powder was dried for 1 d at 80 °C in a vacuum oven at low pressure. Activated MOF-5 nanocrystals were obtained by filtering and washing the powder with a continuous flow of three 30 mL aliquots each of DMF, $CHCl_3$, and acetone in that order. The activated material was dried in a vacuum oven at 240 °C for 1 d at low pressure. MOF-5 was recovered (2.2 g, 80% yield based on Zn) and stored in a capped vial filled with nitrogen.

2.3. Fabrication of MOF-5/Matrimid® mixed-matrix membranes

Flat 0, 10, 20, and 30% (w/w) activated MOF-5/Matrimid® mixed-matrix membranes were fabricated. Two solutions were prepared by dissolving 0.50 g of Matrimid® in 4.50 g of $CHCl_3$ and by dispersing 0.05 g (10%), 0.10 g (20%), or 0.15 g (30%) of activated MOF-5 in 4.5 g of $CHCl_3$. The two solutions were bath sonicated for 4 h and stirred for 1 d and then were mixed by pouring the polymer solution into the MOF-5 solution. The combined solution was stirred and bath sonicated for 1 more hour and then concentrated by purging the excess solvent with a stream of nitrogen until the polymer/$CHCl_3$ concentration reached 10% (w/w). In a laminar flow hood, an AccuLab Jr.™ Drawdown casting table with rod 2.5 was used to cast the membranes onto Mylar® A92 films. The freshly cast membranes were immediately covered with a watch glass to slow solvent evaporation. After 30 min, the watch glass was removed to allow the solvent to evaporate completely. When dried, the membranes were removed from Mylar® and then annealed in a vacuum oven at 240 °C and low pressure for 1 d. After annealing, the membranes were stored in a desiccator filled with nitrogen. The average membrane thickness was 35 μm.

2.4. Characterization

2.4.1. X-ray diffraction, thermogravimetric analysis, surface area, and SEM

Nanocrystal structures of as-synthesized and activated MOF-5, as well as of MOF-5/Matrimid® mixed-matrix membranes, were confirmed by X-ray diffraction with a Rigaku Ultima III diffractometer using Cu Kα X-ray radiation. Thermogravimetric analysis of the MOF-5 nanocrystals and of the mixed-matrix membranes was performed using a PerkinElmer Pyris-1 TGA; the analyses were run in nitrogen from 100 to 1300 °C at a heating rate of 10 °C/min. All TGA analyses were carried out after drying the crystals or annealing the membranes. Nitrogen sorption was performed at liquid nitrogen temperature using Quantachrome's Autosorb-1 instrument. MOF-5 BET surface area and HK pore size were calculated using sample weights after degassing for 1 d at 150 °C. To acquire SEM images, the MOF-5 nanocrystals and the membranes were coated with Au/Pd using a Denton Vacuum Desk II sputter-coater. The coated samples were then imaged using a LEO 1500 series SEM equipped with a field emission gun operated at 10 keV.

2.4.2. Permeation: single gas and gas mixtures

Single gas (N_2, O_2, CH_4, CO_2, and H_2) and gas blend [H_2/CO_2 (75/25, 50/50, 25/75), CH_4/N_2 (94/6, 50/50, 25/75), and CH_4/CO_2 (90/10, 50/50, 25/75)] permeation/separation measurements were carried out using a custom-built permeameter described previously [21,44]. The permeameter is equipped with an MKS PPT-200 quadrupole residual gas analyzer unit (RGA, mass range 1–200 amu) and a leak valve that controls the feed to the RGA. The system (valve actuation, pressure monitoring, gas feed, and data acquisition) is controlled by Labview 7.1 software (National Instruments). In a typical experiment, a 2 cm^2 membrane piece was assembled in a stainless steel cell that exposed one side of the membrane to a pressurized feed (2000 Torr) and the other side to an evacuated line (1 mTorr). The entire system was evacuated for at least 6 h at 35 °C and 1 mTorr before a leak rate test was performed after which permeability experiments were conducted. Ideal selectivities ($\alpha_{i/j}$) were calculated from the ratio of the permeabilities (P, Barrers) of the gases P_i/P_j following the solubility–diffusivity model [45,46]. The determination of P was performed using the last 60% of the pressure–time curve data in the steady state region. The diffusivity, D, was calculated from the relationship $D = \ell^2/6\theta$ where ℓ is the membrane thickness and θ the time-lag. The apparent solubility of the gases in the membrane was calculated from the relationship $S = P/D$ [47–50]. The time lag method for the calculation of diffusivities and solubilities of slow diffusing gases can be reliably used if degassing times are in the range of 4–6θ [51,52]. However, H_2 diffusivity and solubility cannot be calculated reliably with this method due to the short time lag of this gas in the membranes. In this work, a minimum of 4θ membrane degassing times were used before permeation experiments began.

For the compositional analysis of the permeates, the RGA was calibrated according to published procedures and recommendations [53,54] using the mixture standards obtained from Air Liquide. Prior to analysis, the RGA was allowed to reach thermal stability (filament on for at least 2 h) and high vacuum ($<8 \times 10^{-9}$ Torr, measured with an MKS cold cathode gauge). Response curves for H_2/CO_2, CH_4/CO_2, and CH_4/N_2 blends, at different compositions, were obtained by recording the response of the RGA from 1 to 50 amu as a function of the pressure in the RGA chamber, as measured by the cold cathode gauge. Response curves for the pure gases were also recorded. At least 12 RGA scans (four per decade) at pressures ranging from 2×10^{-8} to 1×10^{-6} Torr were recorded for the pure gases and the blends to generate response curves for each composition. Slopes for each gas in the blends at different compositions

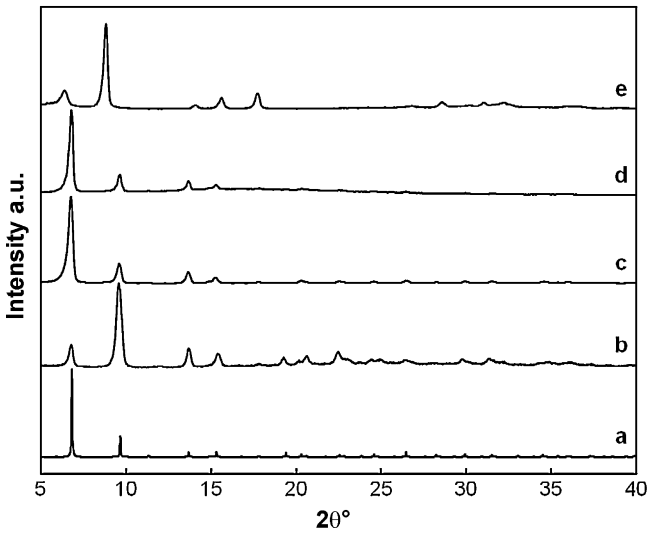

Fig. 3. MOF-5 X-ray diffraction patterns: (a) simulated from single crystal X-ray data [28], (b) as-synthesized, (c) activated, (d) 30% activated MOF-5/Matrimid® mixed-matrix membrane, and (e) activated MOF-5 exposed to moisture.

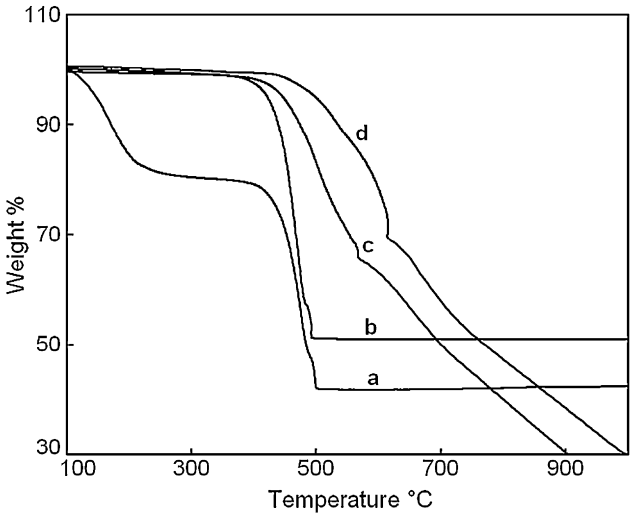

Fig. 4. TGA of (a) as-synthesized MOF-5, (b) activated MOF-5, (c) 20% activated MOF-5/Matrimid® mixed-matrix membrane, and (d) Matrimid® powder.

were calculated using linear regression analysis. The peak intensity at the mass of the intact molecule was used, except in the case of the CH_4/CO_2 blend, where $m/z = 15$ for CH_4 was used due to an interference at $m/z = 16$ from CO_2 fragmentation. The calibration curve for each component of the blend was obtained by performing a linear regression of the slope of the component as a function of its concentration in the blend. Following this procedure, RGA responses for each gas blend tested were acquired and the slope for each gas component of the blend was calculated by linear regression. Then, using the corresponding calibration curve and the calculated slopes, the concentrations of the components in the permeate were determined.

3. Results and discussion

3.1. MOF-5 nanocrystals

X-ray diffraction of as-synthesized and activated MOF-5 nanocrystals (Fig. 3) confirmed that both materials were MOF-5 crystals [28] (Fig. 3a) and that the presumed *hydroxylated* phase (Fig. 3e), that results from the exposure to moisture [36], was not present. Interestingly, X-ray diffraction shows a difference in the intensities of the first two main reflections between the as-synthesized (Fig. 3b) and activated (Fig. 3c) crystals. For the as-synthesized MOF-5 nanocrystals, the reflection at $2\theta = 9.6^\circ$ is more intense than the reflection at $2\theta = 6.7^\circ$ ($I_{6.7^\circ} = 30\% I_{9.6^\circ}$); in the case of the activated MOF-5 nanocrystals, the reflection at $2\theta = 9.6^\circ$ is less intense than the reflection at $2\theta = 6.7^\circ$ ($I_{9.6^\circ} = 20\% I_{6.7^\circ}$). These observations were initially reported by Perez et al. [55] and have been recently confirmed by Hafizovic et al. [56] and Chen and co-workers [35]. It is believed that guest molecules occupy the pores of the as-synthesized crystals [43,57], causing a destructive interference in the XRD pattern and that, through activation, these molecules are removed causing a reverse in the peak intensities.

Thermogravimetric analysis of as-synthesized MOF-5 nanocrystals (Fig. 4a) showed that up to 20% of material is lost at 200 °C, which is attributed to trapped solvent in the pores and to coordination solvent. The crystals remain stable up to 400 °C and, above this temperature, the crystals start to decompose. Activated MOF-5 nanocrystals (Fig. 4b) followed a similar trend except that weight loss began at 400 °C owing to crystal decomposition.

Nitrogen sorption experiments performed on both as-synthesized and activated MOF-5 nanocrystals showed a type I isotherm with pronounced differences in N_2 sorption and BET surface areas: 600 m^2/g for the as-synthesized MOF-5 and 3000 m^2/g for the activated MOF-5 crystals (Fig. 5); the surface area of the activated MOF-5 was in good agreement with previously reported values [29,43]. MOF-5 crystals with surface areas >3000 m^2/g have been referred to as "high quality" crystals owing to their high H_2 storage capacity; the N_2 sorption/desorption isotherm of these crystals does not show a hysteresis loop in contrast to the isotherm of low surface area crystals [35]. Therefore, from Fig. 5 that shows no hysteresis loop and from the high surface area obtained, we can conclude that "high quality" MOF-5 nanocrystals were prepared. The multipoint BET surface area was calculated using the P/P_0 values close to the beginning of the plateau of the isotherm, which corresponds to the formation of a complete monolayer of adsorbed molecules [58]. HK pore size also varies with the activation of the crystals and ranges from 5.3 Å for the as-synthesized MOF-5 nanocrystals to 8.3 Å for the activated MOF-5 nanocrystals. Since the HK method calculates the pore size distribution from the isotherm [59], a variation in pore

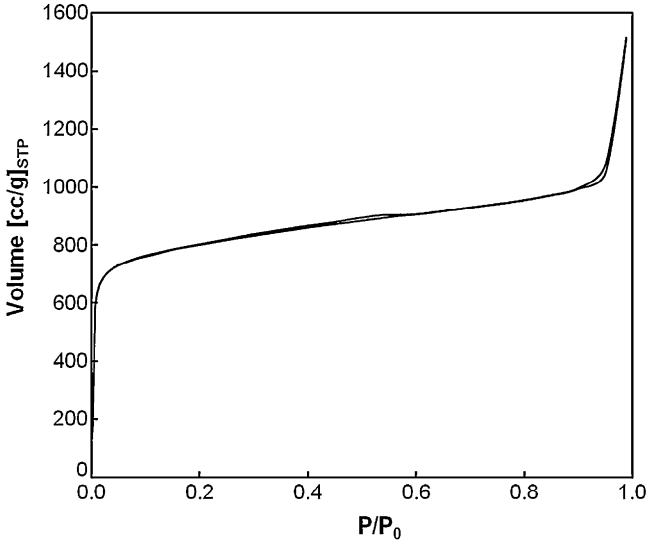

Fig. 5. Nitrogen sorption isotherm at 77 K for activated MOF-5.

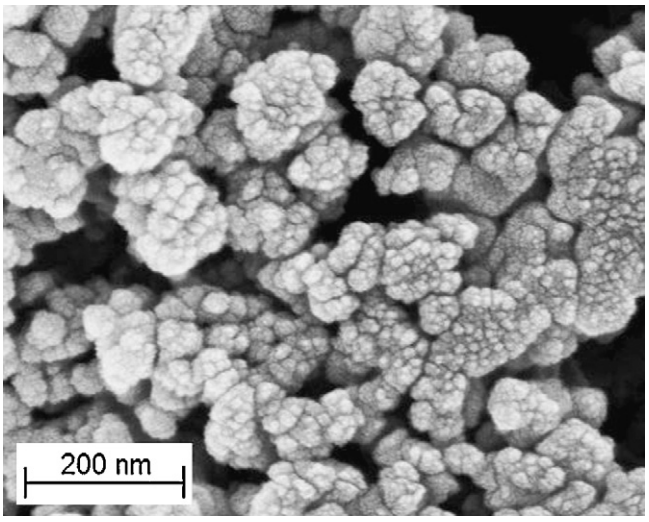

Fig. 6. SEM image of activated MOF-5 nanocrystals; 100 nm particle size.

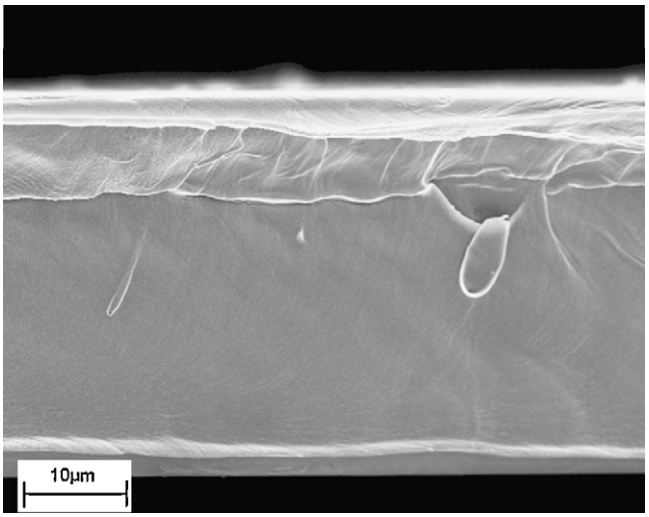

Fig. 7. SEM image of the cross-section of a pure Matrimid® membrane.

size is expected. Physically, the crystal pore size remains constant for both the as-synthesized and activated MOF-5 nanocrystals. However, owing to the presence of guest molecules in the pores of the as-synthesized MOF-5, the amount of N_2 adsorbed is less than that for the activated MOF-5. For the activated MOF-5 crystals, the calculated pore size was 11 Å which is in good agreement with the pore window calculated using Materials Studio® and the published single crystal X-ray data [28].

SEM images showed that the average particle size of both the as-synthesized and activated MOF-5 nanocrystals was 100 nm (Fig. 6) with no defined morphology. Similar SEM images were obtained by Huang et al. [36] which showed no defined crystal morphology with aggregates similar in size (70–90 nm) to the nanocrystals synthesized in this work. Cubic crystals were reported from a solvothermal synthesis [29,43]; however, these crystals were micrometer in size and not suitable for mixed-matrix membrane fabrication. Although strong particle agglomeration of the MOF-5 nanocrystals limited their full dispersion in common organic solvents, even after intensive bath sonication, the obtained dispersion and size reduction of the agglomerates allowed the fabrication of membranes with up to 40% MOF-5 loading. The disadvantages of having agglomerates in the matrix are reflected in poor additive–polymer contact and the formation of non-selective voids. Improved dispersion could be obtained by modifying the organic linker of the crystal to include alkyl chains with functional groups that would make the crystal more compatible with the polymer and the organic solvent. An example of a chemically functionalized MOF is MOP-18 [60] which is soluble in $CHCl_3$, toluene, tetrahydrofuran, and other common organic solvents. Similarly, Rong et al. reported that polystyrene grafted SiO_2 nanoparticles showed good dispersion in benzene, but upon incorporation into a polypropylene matrix, re-agglomeration into micrometer size particles occurred [16]. Currently, we are investigating the effects of this functionalization on membrane fabrication and transport properties with MOP-18 as an additive, and we will be expanding this strategy to other MOFs to improve dispersion.

3.2. MOF-5/Matrimid® mixed-matrix membranes

3.2.1. Membrane characterization

To maximize the interaction between the gas molecules and the MOF sorption sites, only batches of activated MOF-5 nanocrystals that showed high surface area (2500–3000 m^2/g) were used for the fabrication of mixed-matrix membranes with 10, 20, and 30% (w/w) loading. X-ray diffraction patterns of activated MOF-5/Matrimid® mixed-matrix membranes were acquired before and after permeability experiments. In all cases, the diffraction patterns revealed the presence of only one phase corresponding to MOF-5 (see, for example, Fig. 3d). It should also be noted that the relative intensities of the reflections of the MOF-5 in the polymer remained the same ($I_{9.6^\circ}$ = 20% $I_{6.7^\circ}$) as those measured for the pure activated MOF-5 material.

Thermogravimetric analyses of activated MOF-5/Matrimid® membranes (see, for example, Fig. 4c) indicated that there was no loss of weight up to 350 °C (temperature of crystal decomposition) indicating that casting solvent was not trapped in the pores of the MOF-5 nanocrystals. The polymer decomposed above this temperature.

Fig. 7 shows an SEM image of a cross-section of a pure Matrimid® membrane and Fig. 8 shows the surface and cross-sections of 10, 20, and 30% (w/w) MOF-5/Matrimid® mixed-matrix membranes. SEM images of the membrane surfaces (Fig. 8a, d and g) and cross-sections (Fig. 8b, e and h) indicate that there are no gross defects; however, agglomerates of MOF-5 are evident in the polymer. The membrane cross-section morphology reveals the formation of circular cavities and polymer veins (elongated matrix segments) with increased plastic deformation of the polymer (Fig. 8c, f and i). This morphology is an indication of a strong contact/interaction between the polymer and the walls of the MOF-5 nanocrystals, although it is not strong enough to break the agglomerates and keep them dispersed at the primary nanoparticle level. Debonding of the agglomerates from the matrix may be occurring during freeze fracture resulting in the formation of cavities [16,61]. Rigidification of the polymer–additive interface is also expected as a result of the strong interaction of the additive and the matrix, limiting the mobility of the polymer chains [16,61,62]. An example of a morphology with little plastic deformation is that of untreated SiO_2 nanoparticles in polypropylene. Minimal plastic deformation of the matrix–additive interface is observed due to the low affinity of the SiO_2 nanoparticles for the polymer (few polymer veins are observed) [16,61,63].

3.2.2. Gas permeation

Single gas permeation experiments showed that the permeability of all gases increased with MOF-5 loading. For example, at 30% loading the permeability of the resulting membrane increased 120% with respect to the pure polymer cast from the same solvent and tested under the same conditions (our experimental Matrimid®

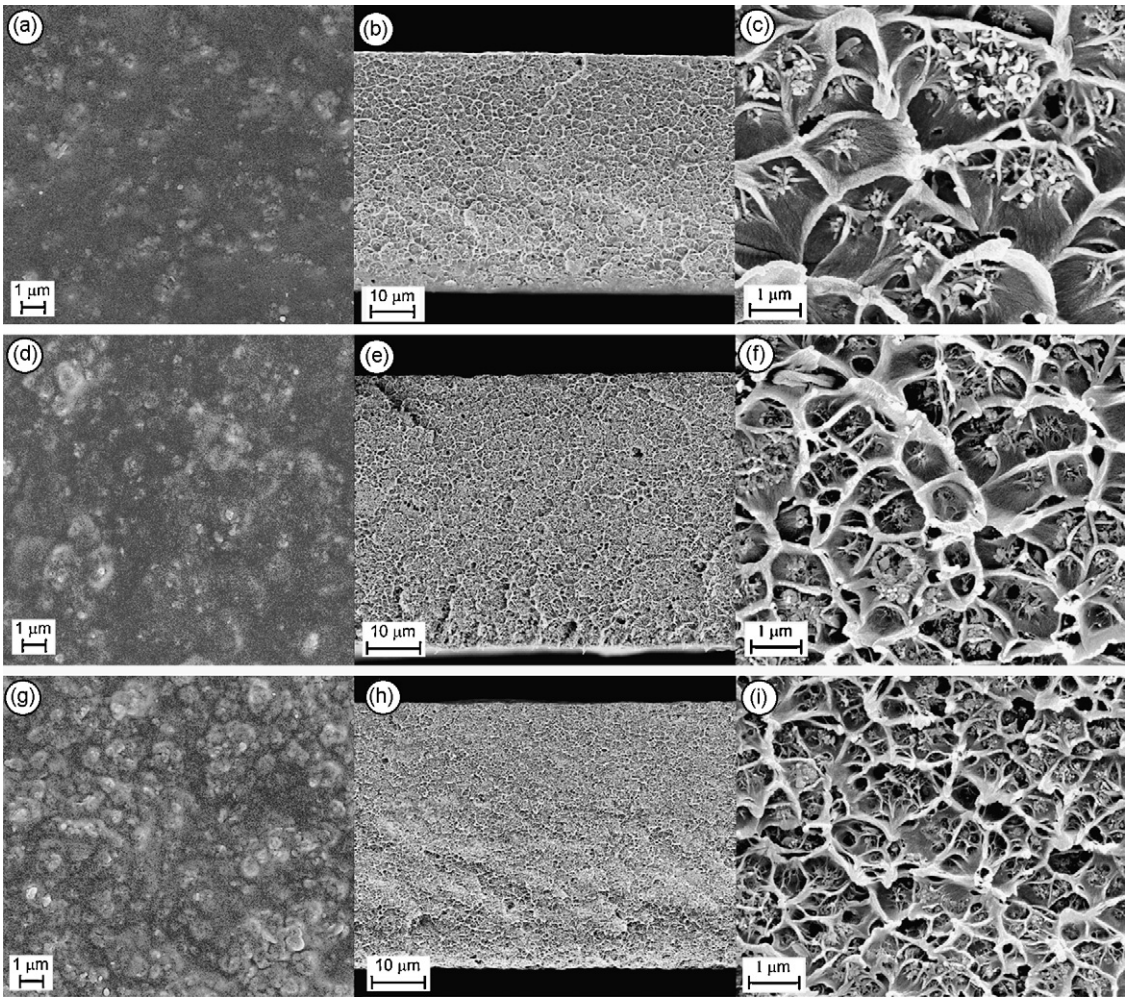

Fig. 8. SEM images of the surface (a, d, and g), cross-section at low magnification (b, e, and h), and cross-section at high magnification (c, f, and i) of 10, 20, and 30% MOF-5/Matrimid® mixed-matrix membranes, respectively. The cross-sections show plastic deformation of the polymer matrix due to the presence of the MOF-5 nanoparticles.

Table 1
Pure gas permeabilities (Barrers) for MOF-5/Matrimid® mixed-matrix membranes at 35 °C and 2 atm.

%MOF-5	P_{H_2}	P_{CO_2}	P_{O_2}	P_{N_2}	P_{CH_4}
0	24.4 ± 0.1	9.0 ± 0.1	1.90 ± 0.01	0.25 ± 0.04	0.22 ± 0.02
10	29.9 ± 4.8	11.1 ± 1.4	2.30 ± 0.30	0.28 ± 0.08	0.22 ± 0.04
20	38.3 ± 8.8	13.8 ± 2.8	2.90 ± 0.60	0.40 ± 0.01	0.34 ± 0.04
30	53.8 ± 3.9	20.2 ± 1.4	4.12 ± 0.37	0.52 ± 0.04	0.45 ± 0.06

permeability values listed in Table 1 agree well with published values [19]). In the case of H_2, an increase in permeability from 24.4 Barrers (Matrimid®) to 53.8 Barrers (30% w/w MOF-5/Matrimid®) was achieved suggesting that the MOF-5 crystals were facilitating gas transport (Table 1). Since the permeabilities of all the gases increased proportionally, the ideal selectivities remained unchanged (Table 2). For example, the H_2/CO_2 separation of pure Matrimid® cast from $CHCl_3$ was 2.70 ($P_{H_2} = 24.4$ Barrers, $P_{CO_2} = 9.0$ Barrers) and, at 30% (w/w) MOF-5 loading, the H_2/CO_2 separation was 2.66 ($P_{H_2} = 53.8$ Barrers, $P_{CO_2} = 20.2$ Barrers). A plot of the facilitation ratios versus the kinetic diameters of the gases (Fig. 9) showed that the ratios increased only with an increase in the MOF-5 loading. To test its resistance to higher pressures, a 20% MOF-5/Matrimid® membrane was run at 3 atm and 35 °C. The permeabilities of the gases tested were identical to the permeabilities of the membrane run at 2 atm and 35 °C ($P^{2\,atm}_{H_2} = 33.3$ Barrers, $P^{3\,atm}_{H_2} = 33.1$ Barrers, $P^{2\,atm}_{CO_2} = 12.6$ Barrers, $P^{3\,atm}_{CO_2} = 11.9$ Barrers, $P^{2\,atm}_{O_2} = 2.6$ Barrers, $P^{3\,atm}_{O_2} = 2.6$ Barrers, $P^{2\,atm}_{N_2} = 0.4$ Barrers, $P^{3\,atm}_{N_2} = 0.4$ Barrers, $P^{2\,atm}_{CH_4} = 0.32$ Barrers, and $P^{3\,atm}_{CH_4} = 0.32$ Barrers). The results also suggest that the membrane is free of non-selective voids.

Table 2
Pure gas ideal selectivities for MOF-5/Matrimid® mixed-matrix membranes at 35 °C and 2 atm.

%MOF-5	α_{H_2/CH_4}	α_{CO_2/CH_4}	α_{O_2/N_2}	α_{H_2/CH_2}	α_{CH_4/N_2}
0	113.0 ± 9.3	41.7 ± 3.3	7.6 ± 1.0	2.71 ± 0.01	0.86 ± 0.06
10	137.4 ± 43.6	51.0 ± 14.6	8.4 ± 1.3	2.68 ± 0.10	0.86 ± 0.37
20	112.0 ± 12.2	40.5 ± 3.5	7.2 ± 1.2	2.76 ± 0.10	0.85 ± 0.07
30	120.0 ± 7.7	44.7 ± 3.0	7 9 ± 0.1	2.66 ± 0.01	0.87 ± 0.05

Gas diffusivities (average of two membranes) of CO_2, O_2, N_2, and CH_4 (Fig. 10) increased with MOF-5 loading; up to 100% increase in diffusivity was observed at 30% MOF-5 loading (D_{CO_2} from 0.44 ± 0.04 to $1.02 \pm 0.07 \times 10^{-8}$ cm^2 s^{-1}, D_{O_2} from 0.94 ± 0.30 to $1.60 \pm 0.07 \times 10^{-8}$ cm^2 s^{-1}, D_{N_2} from 0.19 ± 0.01 to $0.33 \pm 0.03 \times 10^{-8}$ cm^2 s^{-1}, and D_{CH_4} from 0.06 ± 0.01 to $0.12 \pm 0.01 \times 10^{-8}$ cm^2 s^{-1}). The increase in diffusivity can be explained by the porosity introduced by the MOF-5 and by its pore window (0.8 nm), which is larger than the kinetic diameters of the gases tested. In addition to the MOF porosity, the availability of a more uniform surface (crystal wall or linker) for surface

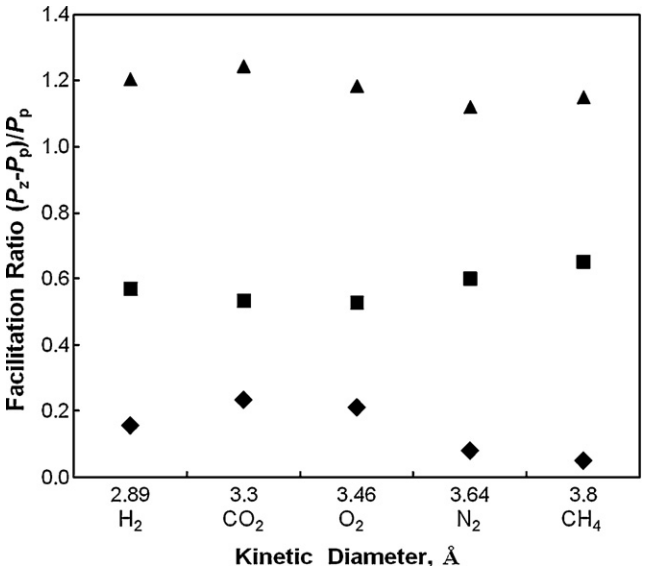

Fig. 9. Facilitation plot of measured gases for MOF-5/Matrimid® mixed-matrix membranes: (♦) 10% MOF-5; (■) 20% MOF-5; (▲) 30% MOF-5.

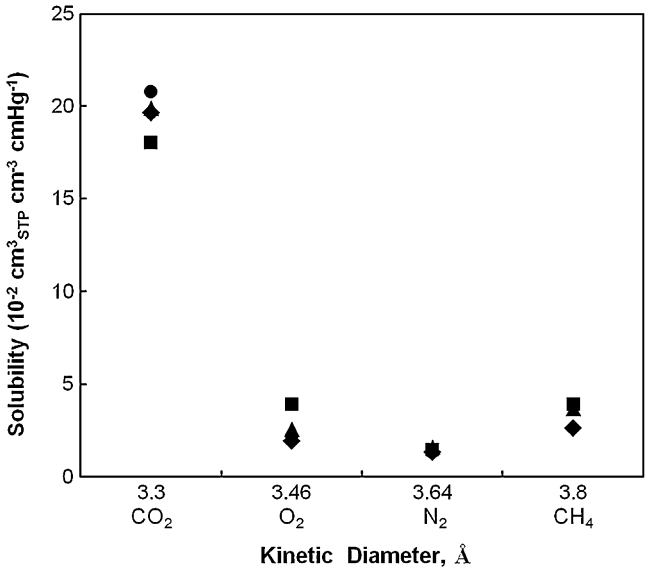

Fig. 11. Solubilities of tested gases for MOF-5/Matrimid® mixed-matrix membranes: (●) Matrimid®; (♦) 10% MOF-5; (■) 20% MOF-5; (▲) 30% MOF-5.

diffusion could help to increase the diffusivity of the gases in the membrane.

Compared to pure Matrimid®, MOF-5/Matrimid® mixed-matrix membranes showed no significant change in solubility with increased MOF-5 loading (Fig. 11). In the case of CO_2, O_2, N_2, and CH_4, the solubility remained essentially unchanged regardless of the MOF-5 loading (S_{CO_2} from 20.70 ± 1.90 to $19.90 \pm 0.05 \times 10^{-2}$ cm^3_{STP} cm^{-3} cmHg, S_{O_2} from 2.20 ± 0.90 to $2.50 \pm 0.12 \times 10^{-2}$ cm^3_{STP} cm^{-3} cmHg, S_{N_2} from 1.30 ± 0.26 to $1.60 \pm 0.02 \times 10^{-2}$ cm^3_{STP} cm^{-3} cmHg, and S_{CH_4} from 3.80 ± 1.30 to $3.70 \pm 0.23 \times 10^{-2}$ cm^3_{STP} cm^{-3} cmHg). These results indicate that the MOF-5 nanocrystals have no significant affinity for CO_2, O_2, N_2, and CH_4 at the temperature and feed pressure used in this study (35 °C and 2 atm). These results agree with Sholl's simulated adsorption isotherms of CO_2, CH_4, and N_2 in MOF-5 which show no significant increase in gas adsorption up to 3–4 atm [40]; only CO_2 adsorption increases at pressures above 3 atm. Therefore, the experimental solubility trends obtained by the time lag method can be considered valid for the gases tested, excluding H_2. It can be concluded, therefore, that the permeability of the gases is enhanced by their increase in diffusivity in the membrane owing to the porosity of the MOF-5. Another example of a non-selective material is MCM-41, which increases the diffusivities but not the solubilities of the gases [21].

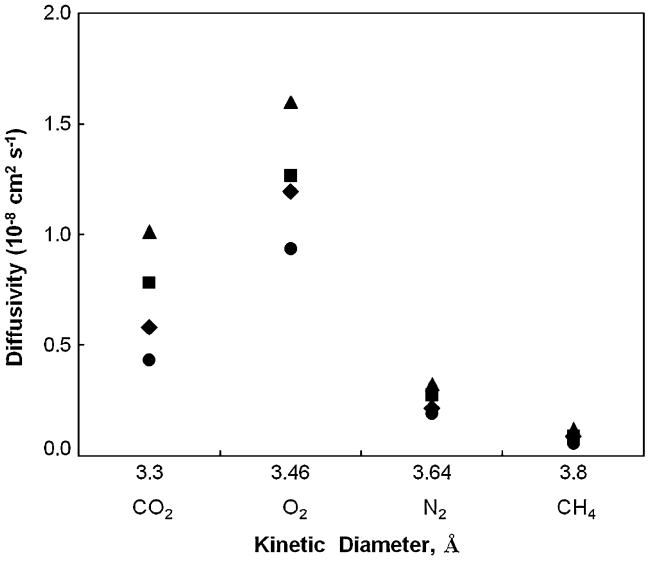

Fig. 10. Diffusivities of tested gases for MOF-5/Matrimid® mixed-matrix membranes: (●) Matrimid®; (♦) 10% MOF-5; (■) 20% MOF-5; (▲) 30% MOF-5.

Although MOF-5 was reported to be a good material for the storage of H_2 [29], selective sorption of gas mixtures in MOFs was not measured until this work for MOF-5 in MMMs. Permeation experiments with blends of gases showed that the separation of H_2/CO_2 in a 30% MOF-5/Matrimid® mixed-matrix membrane did not increase at any feed ratio compared to the separation of the mixtures performed with the pure polymer (Matrimid® $H_2/CO_2 = 2.4$, 30% MOF-5/Matrimid® $H_2/CO_2 = 2.2$). However, the CH_4/N_2 and the CO_2/CH_4 separations showed a selectivity improvement for CH_4 of 15% and 20%, respectively, at a 50/50 feed composition (Table 3). The increased selectivity for methane can be explained in terms of the extended dual mode transport model for gas mixtures that assumes that the primary effect of the presence of more than one gas in the membrane results in the competition between these gases for the fixed unrelaxed free volume in the polymer [64]. Also, the Henry's sorption coefficient of a gas is assumed to be independent of the presence of other components. From this model, it can be concluded that, due to the large solubility of CO_2 in the membrane ($S_{CO_2} = 20.00$, $S_{CH_4} = 1.20 \times 10^{-2}$ cm^3_{STP} cm^{-3} cmHg), the solubility of CH_4 is greatly reduced, rendering CH_4 transport dependent mostly on diffusivity, which is enhanced by the porosity and the uniform surface introduced by the MOF-5 nanocrystals. In addition, the incorporation of MOF-5 reduced the sorption sites in the polymer for CO_2 which contributed to the reduction of CO_2 transport. Pure glassy polyimide, however, showed a different result with increased CO_2 selectivity over CH_4 at different CO_2/CH_4 feed ratios [65]. The increased CO_2 selectivity resulted from an increased CO_2 solubility and a longer residence time of the gas in the polymer leading to a reduced diffusivity of CH_4. Overall, CO_2 dominated the competition for sorption sites in the polymer matrix.

Solubility/diffusivity coupling in mixed gas feeds is mostly observed for glassy polymers and is not yet well understood due to the lack of experimental solubility and diffusivity data for the individual components of the gas mixture. However, it is known that the presence of a second gas in the membrane largely affects the interactions between the gas molecules of the two components and the

Table 3
Separation of gas blends with Matrimid® and 30% MOF-5/Matrimid® mixed-matrix membranes at 35 °C and 2 atm.

Membrane	H_2/CO_2			CO_2/CH_4		CH_4/N_2	
	75/25	50/50	25/75	50/50	10/90	50/50	94/6
Matrimid	2.4 ± 0.3	2.3 ± 0.1	2.5 ± 0.2	38.0 ± 2.0	43.5 ± 1.5	0.82 ± 0.10	0.51 ± 0.05
30% MOF-5/Matrimid	2.2 ± 0.1	2.3 ± 0.2	2.1 ± 0.1	29.0 ± 0.4	38.8 ± 0.5	0.94 ± 0.05	0.50 ± 0.10

polymer resulting in changes in permeability and selectivity, which deviate from the ideal values [65–67].

In the case of the 50/50 and 94/6 CH_4/N_2 mixtures separation with Matrimid® it can be assumed that gas transport follows the solubility–diffusivity model since the membrane is dense. If the separation of the mixture is similar to the ideal selectivity, then it can be assumed that there is no coupling between N_2 and CH_4 diffusivities in the membrane ($\gamma = 0$ not coupled, $\gamma = 1$ strongly coupled). However, the experimental selectivities of Matrimid® for CH_4/N_2 gas mixtures at different feed compositions (Table 3) indicate that there is some degree of coupling ($0 < \gamma \leq 1$) that affects the separation properties of the membrane [65–67].

The immediate effect of the coupling of CH_4 and N_2 diffusivities could be the "pumping" of N_2 by CH_4 since CH_4 has a higher solubility than N_2 in Matrimid® (Fig. 11). This pumping could be high at low N_2 concentration in the feed and decrease with increasing N_2 concentration since the sorption sites for CH_4 are reduced by the presence of N_2 and by the reduction in the ratio of CH_4 to N_2 molecules in the feed that may reduce the coupling effect ($\gamma \rightarrow 0$). The net effect of the pumping of N_2 by CH_4 at low N_2 feed concentration is the increased selectivity for N_2 in the membrane ($CH_4/N_2 = 0.51$ with 94/6 CH_4/N_2). In the case of the 50/50 CH_4/N_2 mixture, the selectivity of the membrane for N_2 is reduced to $CH_4/N_2 = 0.82$.

In the case of the 30% (w/w) MOF-5/Matrimid® membrane, MOF-5 introduces porosity and, therefore, gas transport in the membrane is no longer based solely on solubility and diffusivity in the polymer but also on Knudsen and surface diffusion in the pores and on the walls of the MOF-5 crystals. These new diffusion pathways could promote the decoupling of the CH_4/N_2 diffusivities in favor of CH_4 due to the affinity of MOF-5 for CH_4. The 30% (w/w) MOF-5/Matrimid® MMM shows a 100% increase in CH_4 diffusivity only and a 74% increase in N_2 diffusivity which suggests that MOF-5 may enhance CH_4 transport. In the case of the low N_2 feed concentration (94/6 CH_4/N_2), the coupling effect overcomes the transport and selectivity properties of the MOF-5 resulting in no change in membrane selectivity compared to pure Matrimid®. A different scenario, however, is observed when the N_2 composition of the feed is increased to 50%. In this case, the coupling effect could be weaker allowing the MOF-5 to transport CH_4 more efficiently by surface diffusion and diffusion through the pores since CH_4 molecules can interact better than N_2 with the walls of the MOF resulting in an increase in the selectivity for CH_4.

4. Conclusions

Despite the high surface area of the activated MOF-5, no increase in ideal selectivity for any gas pairs was observed. However, up to a 120% increase in permeability was achieved due to the porosity of the MOF-5 nanocrystals. Gas mixtures (CO_2/CH_4, N_2/CH_4) showed a marked increase in selectivity for CH_4 due to the larger solubility of CO_2 and N_2 in the polymer matrix. This difference in solubility makes CH_4 transport mostly diffusivity dependent and facilitated by the MOF-5 porosity as well as by the uniformity of the surface of its walls. H_2 selectivity remained constant under all gas feed conditions tested.

SEM images of the membrane cross-sections indicate that the increased affinity between the polymer matrix and the MOF-5 nanocrystals increased the plastic deformation of the polymer, inducing the formation of polymer veins (elongated polymer). Additionally, it is also noted that the dispersion of the agglomerates is not complete due to a stronger interaction between the primary nanoparticles than with the polymer, which is manifested in the debonding of the agglomerates and the formation of cavities in the matrix upon freeze fracture. A possible solution to this problem is to functionalize the organic linker of the MOF to increase its compatibility with the polymer. An example of this strategy is MOP-18, a soluble crystal that has an alkylated linker. MOP-18 is soluble in organic solvents and is easily dispersed in the polymer matrix. This type of mixed-matrix membrane is currently under study.

Acknowledgments

The authors thank the U.S. Department of Energy (DOE grant DE-FG26-04NT42173) and the Texas Higher Education Coordinating Board-Advanced Technology Program (ATP grant 009741-0123-2003) for funding this research.

References

[1] L.M. Robeson, Correlation of separation factor versus permeability for polymeric membranes, J. Membr. Sci. 62 (1991) 165.
[2] A.F. Ismail, L.I.B. David, A review on the latest development of carbon membranes for gas separation, J. Membr. Sci. 193 (2001) 1.
[3] A. Julbe, Zeolite membranes—synthesis, characterization and application, in: J. Cejka, H. Bekkum, A. Corma, F. Schuth (Eds.), Introduction to Zeolite Science and Practice, 3rd ed., Elsevier B.V., 2007, p. 181.
[4] S. Li, J.G. Martinek, J.L. Falconer, R.D. Noble, T.Q. Gardner, High-pressure CO_2/CH_4 separation using SAPO-34 membranes, Ind. Eng. Chem. Res. 44 (2005) 3220.
[5] T. Pietraß, Carbon-based membranes, MRS Bull. 31 (2006) 765.
[6] J.M. Van de Graaf, E. Van der Bijl, A. Stol, F. Kapteijn, J.A. Moulijn, Effect of operating conditions and membrane quality on the separation performance of composite silicalite-1 membranes, Ind. Eng. Chem. Res. 37 (1998) 4071.
[7] J. Caro, M. Noack, P. Kölsch, R. Schäfer, Zeolite membranes—state of their development and perspective, Microporous Mesoporous Mater. 38 (2000) 3.
[8] G. Saracco, H.W.J.P. Neomagus, G.F. Versteeg, W.P.M.v. Swaaij, High-temperature membrane reactors: potential and problems, Chem. Eng. Sci. 54 (1999) 1997.
[9] W.J. Koros, R. Mahajan, Pushing the limits on possibilities for large scale gas separation: which strategies? J. Membr. Sci. 175 (2000) 181.
[10] H. Cong, M. Radosz, B.F. Towler, Y. Shen, Polymer–inorganic nanocomposite membranes for gas separation, Sep. Purif. Technol. 55 (2007) 281.
[11] Commonly, MMMs are prepared by dispersing the additive in a polymer matrix followed by casting and annealing. These steps simplify greatly the preparation of MMMs when compared to inorganic membranes. The calculated cost of a 30% (w/w) MOF-5/Matrimid® MMM with a thickness of 30 μm and an area of 1 m^2 is less than US$ 200.
[12] S. Husain, W.J. Koros, Mixed matrix hollow fiber membranes made with modified HSSZ-13 zeolite in polyetherimide polymer matrix for gas separation, J. Membr. Sci. 288 (2007) 195.
[13] S. Shu, S. Husain, W.J. Koros, A general strategy for adhesion enhancement in polymeric composites by formation of nanostructured particle surfaces, J. Phys. Chem. C 111 (2007) 652.
[14] Y. Li, T.S. Chung, C. Cao, S. Kulprathipanja, The effects of polymer chain rigidification, zeolite pore size and pore blockage on polyethersulfone (PES)-zeolite A mixed matrix membranes, J. Membr. Sci. 260 (2005) 45.
[15] T.T. Moore, W.J. Koros, Gas sorption in polymers, molecular sieves, and mixed matrix membranes, J. Appl. Polym. Sci. 104 (2007) 4053.
[16] M.Z. Rong, M.Q. Zhang, Y.X. Zheng, H.M. Zeng, R. Walter, K. Friedrich, Structure–property relationships of irradiation grafted nano-inorganic particle filled polypropylene composites, Polymer 42 (2001) 167.
[17] S.C. Tjong, Structural and mechanical properties of polymer nanocomposites, Mater. Sci. Eng. R 53 (2006) 73.
[18] Y. Li, T.-S. Chung, S. Kulprathipanja, Novel Ag^+-zeolite/polymer mixed matrix membranes with a high CO_2/CH_4 selectivity, AlChE J. 53 (2007) 610.
[19] D.Q. Vu, W.J. Koros, S.J. Miller, Mixed matrix membranes using carbon molecular sieves. I. Preparation and experimental results, J. Membr. Sci. 211 (2003) 311.

[20] T.-S. Chung, L.Y. Jiang, Y. Li, S. Kulprathipanja, Mixed matrix membranes (MMMs) comprising organic polymers with dispersed inorganic fillers for gas separation, Prog. Polym. Sci. 32 (2007) 483.
[21] B.D. Reid, F.A. Ruiz-Trevino, I.H. Musselman, K.J. Balkus Jr., J.P. Ferraris, Gas permeability properties of polysulfone membranes containing the mesoporous molecular sieve MCM-41, Chem. Mater. 13 (2001) 2366.
[22] H. Yehia, T.J. Pisklak, J.P. Ferraris, K.J. Balkus Jr., I.H. Musselman, Methane facilitated transport using copper(II) biphenyl dicarboxylate-triethylenediamine/poly(3-acetoxyethylthiophene) mixed matrix membranes, Polym. Prepr. 45 (2004) 35.
[23] M. Eddaoudi, D.B. Moler, H. Li, B. Chen, T.M. Reineke, M. O'Keeffe, O.M. Yaghi, Modular chemistry: secondary building units as a basis for the design of highly porous and robust metal–organic carboxylate frameworks, Acc. Chem. Res. 34 (2001) 319.
[24] Y. Zhang, I.H. Musselman, J.P. Ferraris, K.J. Balkus Jr., Gas permeability properties of Matrimid® membranes containing the metal–organic framework Cu-BPY-HFS, J. Membr. Sci. 313 (2008) 170.
[25] C.M. Draznieks, J.M. Newsam, A.M. Gorman, C.M. Freeman, G. Férey, De novo prediction of inorganic structures developed through automated assembly of secondary building units (AASBU method), Angew. Chem. Int. Ed. 39 (2000) 2270.
[26] M.M. Davis, J.J. Low, The use of MOFs in pressure swing adsorption, WO 2007/111,738 (2007).
[27] H.K. Chae, D.Y. Siberio-Perez, J. Kim, Y. Go, M. Eddaoudi, A.J. Matzger, M. O'Keeffe, O.M. Yaghi, A route to high surface area, porosity and inclusion of large molecules in crystals, Nature 427 (2004) 523.
[28] M. Eddaoudi, J. Kim, N. Rosi, D. Vodak, J. Wachter, M. O'Keeffe, O.M. Yaghi, Systematic design of pore size and functionality in isoreticular MOFs and their application in methane storage, Science 295 (2002) 469.
[29] O.M. Yaghi, N.L. Rosi, J. Eckert, M. Eddaoudi, D.T. Vodak, J. Kim, M. O'Keeffe, Hydrogen storage in microporous metal–organic frameworks, Science 300 (2003) 1127.
[30] K. Seki, Design of an adsorbent with an ideal pore structure for methane adsorption using metal complexes, Chem. Commun. (2001) 1496.
[31] R. Matsuda, R. Kitaura, S. Kitagawa, Y. Kubota, R.V. Belosludov, T.C. Kobayashi, H. Sakamoto, T. Chiba, M. Takata, Y. Kawazoe, Y. Mita, Highly controlled acetylene accommodation in a metal–organic microporous material, Nature 436 (2005) 238.
[32] D. Tanaka, S. Kitagawa, Captured molecules in coordination frameworks, MRS Bull. 32 (2007) 540.
[33] S. Kitagawa, S.I. Norob, T. Nakamura, Pore surface engineering of microporous coordination polymers, Chem. Commun. (2006) 701.
[34] S.S. Kaye, A. Dailly, O.M. Yaghi, J.R. Long, Impact of preparation and handling on the hydrogen storage properties of $Zn_4O(1,4\text{-benzenedicarboxylate})_3$ (MOF-5), J. Am. Chem. Soc. 129 (2007) 14176.
[35] C.S. Tsao, M.S. Yu, T.Y. Chung, H.C. Wu, C.Y. Wang, K.S. Chang, H.L. Chen, Characterization of pore structure in metal–organic framework by small-angle X-ray scattering, J. Am. Chem. Soc. 129 (2007) 15997.
[36] L. Huang, H. Wang, J. Chen, Z. Wang, J. Sun, D. Zhao, Y. Yan, Synthesis, morphology control, and properties of porous metal–organic coordination polymers, Microporous Mesoporous Mater. 58 (2003) 105.
[37] J.L.C. Rowsell, J. Eckert, O.M. Yaghi, Characterization of H_2 binding sites in prototypical metal–organic frameworks by inelastic neutron scattering, J. Am. Chem. Soc. 127 (2005) 14904.
[38] T. Sagara, J. Klassen, E. Ganz, Computational study of hydrogen binding by metal–organic framework-5, J. Chem. Phys. 121 (2004) 12543.
[39] T. Sagara, J. Klassen, J. Ortony, E. Ganz, Binding energies of hydrogen molecules to isoreticular metal–organic framework materials, J. Chem. Phys. 123 (2005) 014701.
[40] A.I. Skoulidas, D.S. Sholl, Self-diffusion and transport diffusion of light gases in metal–organic framework materials assessed using molecular dynamics simulations, J. Phys. Chem. B 109 (2005) 15760.
[41] H. Li, M. Eddaoudi, M. O'Keeffe, O.M. Yaghi, Design and synthesis of an exceptionally stable and highly porous metal–organic framework, Nature 402 (1999) 276.
[42] J.L.C. Rowsell, A.R. Millward, K.S. Park, O.M. Yaghi, Hydrogen sorption in functionalized metal–organic frameworks, J. Am. Chem. Soc. 126 (2004) 5666.
[43] T. Mueller, M. Schubert, F. Teich, H. Puetter, K. Schierle-Arndt, J. Pastre, Metal–organic-frameworks-prospective industrial applications, J. Mater. Chem. 16 (2005) 626.
[44] S. Riley, Gas permeability and selectivity studies of pure poly(3-[2,5,8-trioxynonyl]thiophene), PTONT, and PTONT/poly(ethylene oxide) polymer blend membranes, Ph.D. Dissertation, The University of Texas at Dallas, Richardson, TX, 2000.
[45] K. Ghosal, B.D. Freeman, Gas separation using polymer membranes: an overview, Polym. Adv. Technol. 5 (1993) 673.
[46] W.J. Koros, G.K. Fleming, Membrane-based gas separation, J. Membr. Sci. 83 (1993) 1.
[47] R.M. Felder, Estimation of gas transport coefficients from differential permeation, integral permeation, and sorption rate data, J. Membr. Sci. 3 (1978) 15.
[48] H.L. Frisch, The time lag in diffusion, J. Phys. Chem. 61 (1957) 93.
[49] I. Kresse, A. Usenko, J. Springer, V. Privalko, Gas transport properties of soluble poly(amide imide)s, J. Polym. Sci. B: Polym. Phys. 37 (1999) 2183.
[50] R. Ash, A note on generalised time-lags, J. Membr. Sci. 270 (2006) 196.
[51] P. Galiatsatou, N.K. Kanellopoulos, J.H. Petropoulos, Characterization of the transport properties of membranes of uncertain macroscopic structural homogeneity, J. Membr. Sci. 280 (2006) 634.
[52] W.J. Koros, D.R. Paul, A.A. Rocha, Carbon dioxide sorption and transport in polycarbonate, J. Polym. Sci.: Polym. Phys. Ed. 14 (1976) 687.
[53] J.A. Basford, M.D. Boeckmann, R.E. Ellefson, A.R. Filippelli, D.H. Holkeboer, L. Lieszkovsky, C.M. Stupak, Recommended practice for the calibration of mass spectrometers, J. Vac. Sci. Technol. A 11 (1993) A22.
[54] W.G. Bley, Quantitative measurements with quadrupole mass spectrometers: important specifications for reliable measurements, Vacuum 38 (1988) 103.
[55] E.V. Perez, K.J. Balkus Jr., J.P. Ferraris, I.H. Musselman, Mixed-matrix membranes for gas separation using metal–organic frameworks, PMSE Prepr. 95 (2006) 815.
[56] J. Hafizovic, M. Bjorgen, U. Olsbye, P.D.C. Dietzel, S. Bordiga, C. Prestipino, C. Lamberti, K.P. Lillerud, The inconsistency in adsorption properties and powder XRD data of MOF-5 is rationalized by framework interpenetration and the presence of organic and inorganic species in the nanocavities, J. Am. Chem. Soc. 129 (2007) 3612.
[57] A.R. Millward, O.M. Yaghi, Metal–organic frameworks with exceptionally high capacity for storage of carbon dioxide at room temperature, J. Am. Chem. Soc. 127 (2005) 17998.
[58] S. Brunauer, P.H. Emmett, E. Teller, Adsorption of gases in multimolecular layers, J. Am. Chem. Soc. 60 (1938) 309.
[59] G. Horvath, K. Kawazoe, Method for the calculation of effective pore size distribution in molecular sieve carbon, J. Chem. Eng. Jpn. 16 (1983) 470.
[60] H. Furukawa, J. Kim, K.E. Plass, O.M. Yaghi, Crystal structure, dissolution, and deposition of a 5 nm functionalized metal–organic great rhombicuboctahedron, J. Am. Chem. Soc. 128 (2006) 8398.
[61] M.Q. Zhang, M.Z. Rong, H.B. Zhang, K. Friedrich, Mechanical properties of low nano-silica filled high density polyethylene composites, Polym. Eng. Sci. 43 (2003) 490.
[62] M. Zhang, M. Rong, K. Friedrich, Application of non-layered nanoparticles in polymer modification, in: Polymer Composites, Springer, US, 2005, p. 25.
[63] M.Z. Rong, M.Q. Zhang, S.L. Pan, B. Lehmann, K. Friedrich, Analysis of the interfacial interactions in polypropylene/silica nanocomposites, Polym. Int. 53 (2004) 176.
[64] W.J. Koros, Model for sorption of mixed gases in glassy polymers, J. Polym. Sci.: Polym. Phys. Ed. 18 (1980) 981.
[65] S.S. Dhingra, E. Marand, Mixed gas transport study through polymeric membranes, J. Membr. Sci. 141 (1998) 45.
[66] A.M. Simon, P. Doran, R. Paterson, Assessment of diffusion coupling effects in membrane separation. Part I. Network thermodynamics modelling, J. Membr. Sci. 109 (1996) 231.
[67] E.A. Mason, L.F. del Castillo, R.F. Rodríguez, Coupling-constant description of coupled flow and diffusion, J. Membr. Sci. 74 (1992) 253.